CityU
香港城市大學
City University of Hong Kong
專業 創新 胸懷全球
Professional·Creative
For The World

CityU Scholars

# Na2SeO3
## A Na-Ion Battery Positive Electrode Material with High Capacity

Su, Bizhe; Zhang, Jiaolong; Fujita, Manabu; Zhou, Wenchong; Sit, Patrick H.-L.; Yu, Denis Y. W.

**Published in:**
Journal of the Electrochemical Society

**Published: 01/01/2019**

**Document Version:**
Final Published version, also known as Publisher's PDF, Publisher's Final version or Version of Record

**License:**
CC BY

**Publication record in CityU Scholars:**
Go to record

**Published version (DOI):**
10.1149/2.0131903jes

**Publication details:**
Su, B., Zhang, J., Fujita, M., Zhou, W., Sit, P. H-L., & Yu, D. Y. W. (2019). $Na_2SeO_3$: A Na-Ion Battery Positive Electrode Material with High Capacity. *Journal of the Electrochemical Society*, *166*(3), A5075-A5080. https://doi.org/10.1149/2.0131903jes

**Citing this paper**
Please note that where the full-text provided on CityU Scholars is the Post-print version (also known as Accepted Author Manuscript, Peer-reviewed or Author Final version), it may differ from the Final Published version. When citing, ensure that you check and use the publisher's definitive version for pagination and other details.

**General rights**
Copyright for the publications made accessible via the CityU Scholars portal is retained by the author(s) and/or other copyright owners and it is a condition of accessing these publications that users recognise and abide by the legal requirements associated with these rights. Users may not further distribute the material or use it for any profit-making activity or commercial gain.

**Publisher permission**
Permission for previously published items are in accordance with publisher's copyright policies sourced from the SHERPA RoMEO database. Links to full text versions (either Published or Post-print) are only available if corresponding publishers allow open access.

**Take down policy**
Contact lbscholars@cityu.edu.hk if you believe that this document breaches copyright and provide us with details. We will remove access to the work immediately and investigate your claim.

Download date: 06/12/2021

JES Focus Issue of Selected Papers from IMLB 2018

# $Na_2SeO_3$: A Na-Ion Battery Positive Electrode Material with High Capacity

**Bizhe Su,[1] Jiaolong Zhang,[2] Manabu Fujita,[3] Wenchong Zhou,[1] Patrick H.-L. Sit,[1] and Denis Y. W. Yu [1,z]**

[1] *School of Energy and Environment, City University of Hong Kong, Hong Kong*
[2] *Engineering Laboratory for the Next Generation Power and Energy Storage Batteries, Graduate School at Shenzhen, Tsinghua University, Shenzhen, People's Republic of China*
[3] *Toray Advanced Materials Research Laboratories (China) Co., Ltd. (TARC), People's Republic of China*

Recent experimental and theoretical studies on the family of Li-rich layered materials show that they can deliver much higher capacities than traditional Li-transitional metal oxides. This also leads to great interests in Na-rich layered oxides as alternative positive electrode materials for sodium-ion batteries for large-scale energy storage. Herein, we report a Na-rich material, $Na_2SeO_3$ with an unconventional layered structure as a positive electrode material in NIBs for the first time. This material can deliver a discharge capacity of 232 mAh $g^{-1}$ after activation, one of the highest capacities from sodium-based positive electrode materials. X-ray photoelectron spectroscopy indicates the oxidation state of selenium remains unchanged during the charge process. Theoretical simulation shows that after removal of Na, spin is situated around oxygen atoms near the Na vacancy, and the projected density of state of oxygen electron is close to the Fermi level. These suggest the involvement of oxygen during charge-discharge. This work will propel new searches of high-capacity sodium-based positive electrode materials.
© The Author(s) 2018. Published by ECS. This is an open access article distributed under the terms of the Creative Commons Attribution 4.0 License (CC BY, http://creativecommons.org/licenses/by/4.0/), which permits unrestricted reuse of the work in any medium, provided the original work is properly cited. [DOI: 10.1149/2.0131903jes]

Manuscript submitted August 20, 2018; revised manuscript received October 26, 2018. Published November 21, 2018. *This paper is part of the JES Focus Issue of Selected Papers from IMLB 2018.*

Due to the intermittence of most renewable energies such as wind, solar and tide, an effective energy-storage system is required to integrate them into power grids to improve the energy-utilization rate.[1,2] Li-ion batteries (LIBs) have attracted the most interests because of its high energy density and success in portable electronics applications. However, the uneven geographical distribution and high cost of lithium hinder its application in large-scale energy storage systems. Sodium, which is in the same group as lithium in the periodic table with similar physical properties, shows its advantages in cost and abundance and holds promise for the energy storage in grid scale. In addition, Na-ion batteries (NIBs) show many similarities with LIBs, so previous knowledges from LIBs can help the development of NIBs.[3–5]

Developments of positive electrode materials with high energy density and good cyclability are crucial for the commercialization of NIBs. Currently, research interests are mainly focused on polyanionic compounds such as $Na_3V_2(PO_4)_3$,[6] $Na_3V_2(PO_4)_2F_3$[7] with a longer cycle life, and as well P2- $Na_{2/3}Ni_{1/3}Mn_{2/3}O_2$[8] and O3- $NaNi_{0.5}Mn_{0.5}O_2$[9] layered oxides. Though, the typical capacities are below 150 mAh $g^{-1}$. Recent works on $Na_3RuO_4$,[10] $Na_2IrO_3$,[11] $Na_{2/3}[Mg_{0.28}Mn_{0.72}]O_2$,[12] $NaVO_3$[13] have shown oxygen participation during charge/discharge, and most of them are analogous to the Li-excess layered oxides $Li_2MnO_3$ family which can deliver a high discharge capacity of more than 250 mAh $g^{-1}$ in LIB.[14–17] This suggests that there may be alternative ways to increase capacity of positive electrode materials for NIB.

In this work, we start with the formula $Na_2MO_3$ and ask whether there are materials other than M = Ru and Ir that can be charged to give a high capacity. We came across $Na_2SeO_3$, a highly-covalent compound with an unconventional structure, that can be activated beyond 4.5 V vs. $Na/Na^+$ to give a high reversible capacity of 232 mAh $g^{-1}$ when discharged to 1.5 V vs. $Na/Na^+$. This is the first report of such a positive electrode material for NIBs, and the obtained capacity is also one of the largest amongst NIB positive electrodes. During charge and discharge, a given capacity only reflects the number of electrons that can be extraction from or inserted into a material. The actual charge transfer can be accommodated by the change in oxidation state of different elements in the material. Despite the large capacity, X-ray photoelectron spectrscopy measurements indicate that the oxidation state of Se (at least on the surface) remains the same during charging. This suggests there are other contributions to charge transfer. The competing reaction between cationic and anionic redox can be analyzed theoretically by calculating the density of states (DOS) of the O 2p state and metal 3d/4d (or non-metal 3p/4p) state.[10,18] The calculated energy of the oxygen is closer to the Fermi level than that of Se in $Na_xSeO_3$, inferring some oxygen reaction in the material. Further work is necessary to fully understand the reaction mechanism of the material. Cycle stability of the material is poor at the moment due to structural change and possibly selenium dissolution from the material. A few methods such as coating or doping to stabilize the material are suggested.

## Experimental

***Material preparation and characterizations.***—To synthesis $Na_2SeO_3$, $SeO_2$ (Aladdin, 98%) and NaOH (Sigma-aldrich, 98%) with a mole ratio of 1:2 was dissolved in deionized water. Then the solution was heated at 90°C for 10 hrs in a vacuum oven to evaporate the water, followed by annealing at a higher temperature of 150°C for 10 hrs in the vacuum oven. Synthetic $Na_2SeO_3$ is stable in air. Some samples were further ball-milled with acetylene black (AB) in a weight ratio of 3:1 at 300 rpm for 2 hrs in ethanol to increase its electrical conductivity (denoted as BM-$Na_2SeO_3$). The crystal structure of the as-prepared samples were determined by X-ray diffraction (X'Pert3 Powder X-ray Diffractiometer, PANalytical). The morphology of samples were characterized by scanning electron microscopy (EVO MA10, Zeiss). The surface analysis of electrodes for X-ray photoelectron spectroscopy (XPS) measurements was carried out with a K-Alpha+ spectrometer (ThermoFisher Scientific). All electrodes for ex-situ tests were washed three times with dimethyl carbonate (DMC) and placed in a specific vacuum holder in an Ar-filled glove box to avoid exposing to air. Raman measurements were carried out by using a 633 nm laser with a Raman microscope (Renishaw, Invia Raman).

***Assembly of cells and electrochemical characterizations.***—Active material was mixed with AB and polyvinylidene fluoride (PVdF) with a weight ratio of 6:2:2 in 1-methyl-2-pyrrolidone (NMP) to form a slurry. For the BM-$Na_2SeO_3$ sample, only PVdF is added during

[z] E-mail: denisyu@cityu.edu.hk

Downloaded on 2019-07-17 to IP 144.214.124.11 address. Redistribution subject to ECS terms of use (see ecsdl.org/site/terms_use) unless CC License in place (see abstract).

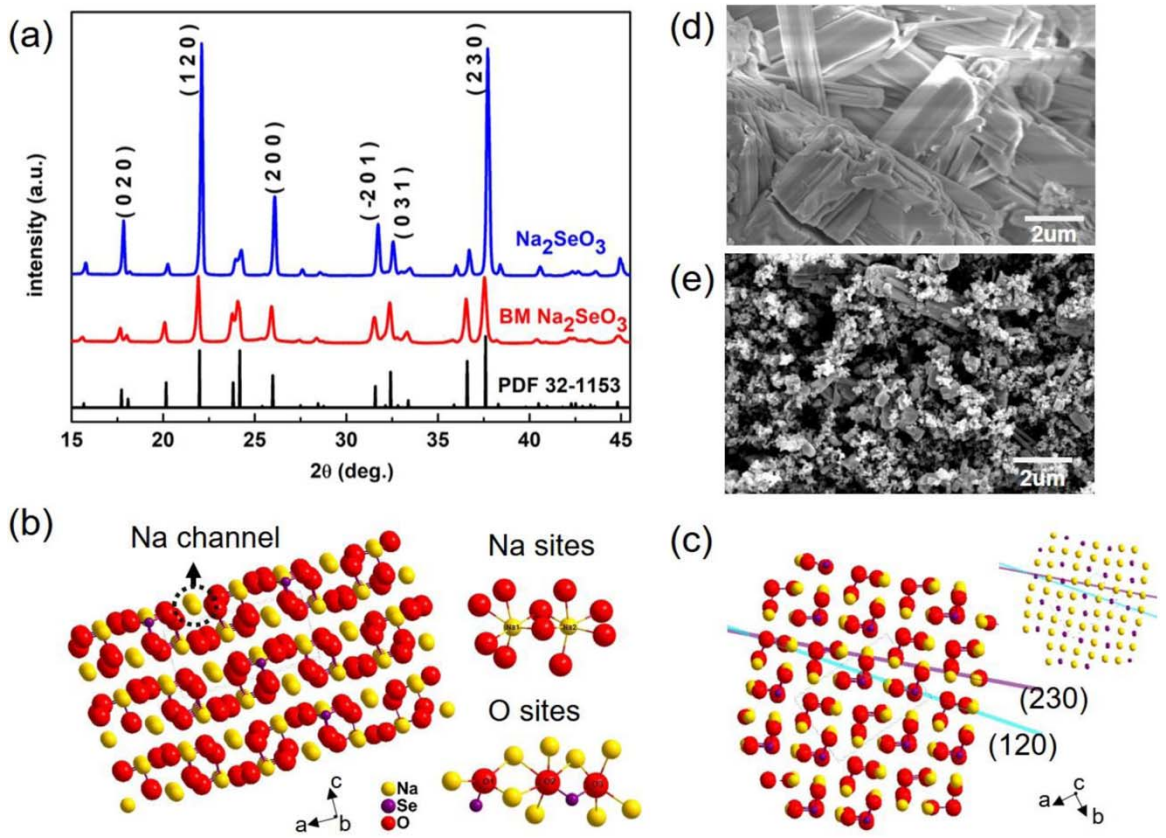


**Figure 1.** (a) XRD patterns of $Na_2SeO_3$ and BM-$Na_2SeO_3$ powder; (b) Crystal structure of $Na_2SeO_3$ from [010] direction and environment of Na sites and O sites; (c) Crystal structure of $Na_2SeO_3$ from [001] direction; (d) SEM of $Na_2SeO_3$ powder; (e) SEM of BM-$Na_2SeO_3$ powder.

slurry making. The slurry was then coated with a doctor blade onto aluminum foil and dried at 80°C. 16 mm diameter discs were cut out and then pressed by a calender to a packing density of $1.2 \pm 0.1$ mg $cm^{-3}$. 2032-type coin cells were made in an argon-filled glove box with Na metal as counter electrode, glass fiber filter as separator and 1M $NaPF_6$ in propylene carbonate (PC) with 5 vol% fluoroethylene carbonate (FEC) as electrolyte. The coin cells were galvanostatically charged/discharged using a battery tester (Neware) at 22°C.

***Theoretical calculation method.—***To study the charge transfer mechanism, we calculated the spin density for the $Na_2SeO_3$ system after Na removal using density functional theory (DFT) calculation,[19,20] which is implemented in the Plane-Wave Self-Consistent Field (PWscf) module of the Quantum Espresso (QE) Package.[21] For the exchange-correlation and electron-ionic core interactions, the generalized gradient approximations (GGA) Perdew-Burke-Ernzerhof (PBE) functional[22] and the ultrasoft pseudopotentials (USPP)[23] were employed in this work, respectively. For the wavefunctions and the augmented charge density, the plane wave kinetic energy cutoffs of 35 Ry and 350 Ry were found accurate enough to ensure the accuracy of calculation. All calculations are spin-polarized. Since the $Na_2SeO_3$ adopts a monoclinic crystal structure, the geometry relaxation and spin density calculations were carried out for the same phase structure with supercell lengths of a = 4.91 Å, b = 10.00 Å and c = 6.85 Å and cell angles of $\alpha = 90.0°$, $\beta = 91.1°$, and $\gamma = 90.0°$. Correspondingly, with Monkhorst-Pack scheme, a k-point sampling mesh of $4 \times 2 \times 3$ for the a monoclinic cell was used.

## Results and Discussion

***Physical characterization.—***The as-prepared powder is white in color and its X-ray diffraction pattern is shown in Fig. 1a. As observed, all of Bragg diffraction peaks of the synthesized and ball-milled samples coincide nicely to $Na_2SeO_3$ with a space group of $P2_1/c$ (PDF card No. 32-1153) without any impurity phases. The material shows a monoclinic structure consisting of two different [$NaO_6$] octahedras and [$SeO_3$] pyramids which are linked together through their edges (Fig. 1b), while oxygen atoms are in three different sites surrounded by one Se and different amount of Na atoms (3, 4, 5)(Fig. 1b). This arrangement could create a flexible and beneficial environment for O to rotate and form peroxo species with neighboring O.[24] Na atoms are in two different octahedron sites which make Na much easier to migrate in comparison to tetrahedron or hexahedron sites (Fig. 1b). A fitting of the XRD data gives a lattice constant of a = 4.899(27) Å, b = 9.992(1) Å, c = 6.848(4) Å, $\beta = 90.95°$, consistent with previous report.[25] Particularly, the highest Bragg diffraction peaks of the as-prepared $Na_2SeO_3$ powder corresponds to the (120) and (230) planes, which indicates that [120] and [230] directions may be the preferred orientation of the crystals. As shown from Fig. 1c, there are also 1D Na channels after removing all oxygen atoms from unit cells in the direction of [001] which is perpendicular to the main crystal growth orientations [120] and [230]. Meanwhile, primary particle of as-prepared $Na_2SeO_3$ shows a large rod-like shapes with length of about 5 μm (Fig. 1d). After ball milling with AB, the diffraction peaks of BM-$Na_2SeO_3$ decreases slightly, and the particle size decreases to ~1 μm as observed in Fig. 1e.

***Electrochemistry.—***The charge-discharge profiles of $Na_2SeO_3$ and BM-$Na_2SeO_3$ are obtained with a galvanostatic cycling at 10 mA $g^{-1}$ between 1.5 and 4.7 V versus $Na^+$/Na. If the $Na_2SeO_3$ is discharged initially to 1.5 V after cell assembly, no capacity is obtained. This suggests that $Na_2SeO_3$ is inactive as an anode material (i.e. no electrochemical reaction to accommodate extra Na in the structure) down to 1.5 V. However, when it is firstly charged to 4.7 V, a voltage plateau at nearly 4.5 V with a capacity of 360 mAh $g^{-1}$ is obtained,

Downloaded on 2019-07-17 to IP 144.214.124.11 address. Redistribution subject to ECS terms of use (see ecsdl.org/site/terms_use) unless CC License in place (see abstract).

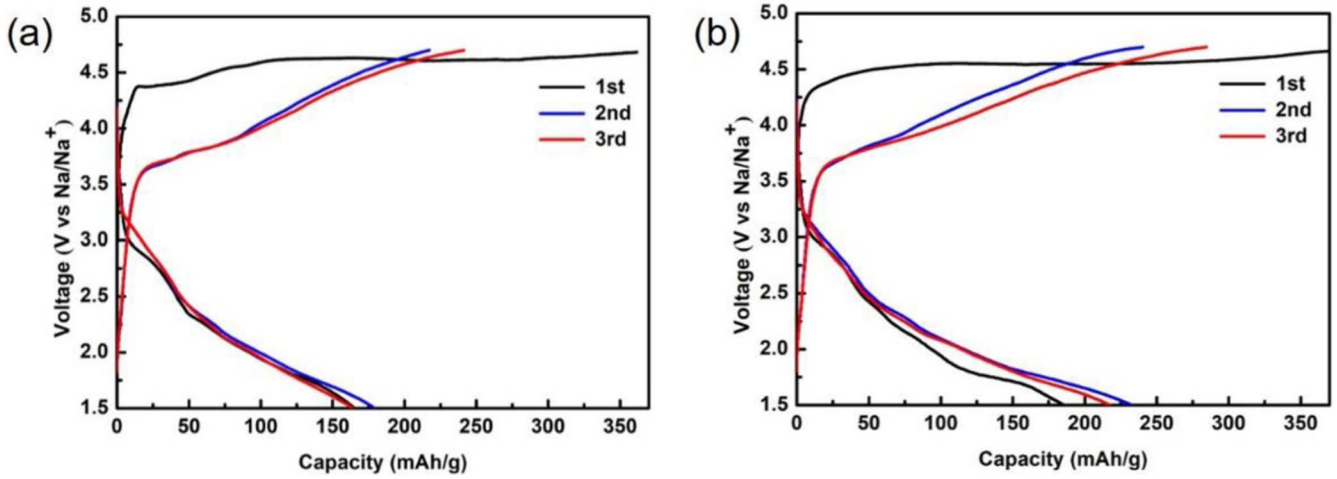


**Figure 2.** Fist, second and third charge-discharge curves of (a) $Na_2SeO_3$ and (b) BM-$Na_2SeO_3$ between 1.5–4.7 V at 10 mA $g^{-1}$.

as shown in Fig. 2a. Since the theoretical capacity of $Na_2SeO_3$ is 310 mAh $g^{-1}$ based on 2 Na transfer, part of the large charge capacity probably originates from electrolyte decomposition at high voltage. When the electrode is then discharged to 1.5 V, a high reversible capacity of 163 mAh $g^{-1}$ is obtained. The voltage plateau at 4.5 V only appears during first charge, and the charging curves shift down to lower potential between 3.5 V and 4.7 V in subsequent cycles. On the other hand, discharge behaviors in the following cycles are consistent with the first cycle, and capacity reaches its maximum at 2$^{nd}$ cycle with 178 mAh $g^{-1}$. The charge-discharge behavior of $Na_2SeO_3$ resembles that of $Li_2MnO_3$,[16] which also requires a high-voltage charging to activate the oxygen redox reaction to obtain high capacity. This suggests that $Na_2SeO_3$ may share similar mechanism with $Li_2MnO_3$.

BM-$Na_2SeO_3$ shows similar charge-discharge behavior (see Fig. 2b). Ball milling the material with carbon increases its reversible capacity to 232 mAh $g^{-1}$, one of the highest values reported for Na-ion positive electrode materials. The improvement is attributed to smaller particle size and improved electrical conductivity with better contact with conductive materials after ball milling.

In order to understand the charge-discharge mechanism of $Na_2SeO_3$, the evolution of the selenium valence state in the pristine, charged, and discharged electrodes were investigated by XPS (Fig. 3). The results are collated with data from National Institute of Standards and Technology XPS Database 20, Version 4.1.[26] The as-prepared electrode (black curve) shows a $3d_{5/2}$ peak of Se at a binding energy of 59.25 eV, consistent to those reported as $Na_2SeO_3$. After initial charge to 4.7 V (red curve), the $3d_{5/2}$ peak of Se shifts slightly toward a higher energy of 59.5 which is still regarded as $Na_2SeO_3$.[26] No apparent oxidation on $Se^{4+}$ could indicate involvement of oxygen redox reaction. Besides, peak intensity of Na 2s decreases because of Na extraction. After initial discharge to 1.5 V (blue curve), the XPS peak of Se as $Na_2SeO_3$ remains the same while the peak intensity of Na 2s increaes because of Na insertion. Interestingly, peaks corresponding to Se-Se at 55.6 eV and 56.25 eV become visible, indicating the formation of selenium-like material after discharge process.

To further study the initial oxidation process of $Na_2SeO_3$, theoretical calculations on the spin density and the density of states (DOS) of $Na_2SeO_3$ with DFT were conducted. To obtain the spin density, we first calculated the electronic densities for the spin-up and spin-down electrons form the DFT Kohn-Sham orbitals. The spin density was calculated from the difference between the spin-up and spin-down electronic densities. The projected density of states (PDOS) for different atoms were calculated by projecting the DFT Kohn-Sham orbitals onto the atomic orbitals of the concerned atoms. As shown in Fig. 4, there is no spin on any of the atoms in the unit cell for $Na_8Se_4O_{12}$. Moreover, the O 2p electrons were found to dominate the vicinity of the Fermi level from the DOS plots. After the removal of one Na (x = 7), spin is shown around oxygen atoms near the vacancy. Continuing removal of one more Na (x = 6) leads to more spin around the oxygen atoms, though some spin starts to appear around Se, which is consistent to a small shift of the Se peak to higher energy in XPS. Also, the density of states of the oxygen atoms overlaps with Fermi level which suggests oxide ions are responsible for charge compensation. Even though the structure of the material gradually changes to amorphous with de-sodiation (as discussed later), we expect the DFT calculation using a monoclinic structure is still valid at the initial state of the de-sodiation.

Our results hint at some contributions of oxygen redox reaction during charge and discharge, similar to that in $Li_2MnO_3$. We hypothesize that during charging, sodium is removed from the $Na_2SeO_3$ structure with some oxygen oxidation reaction near 4.5 V, accompanied with the formation of [$SeO^{x-}{}_3$] (x<2) product. During the discharge process, sodium returns to the material, together with some oxygen reduction reaction and also the formation of Se from $Se^{4+}$. Direct measurements, in particular, on the state of the oxygen during charge and discharge and the amount of oxygen released from the material will be necessary to further elucidate the reaction mechanism.

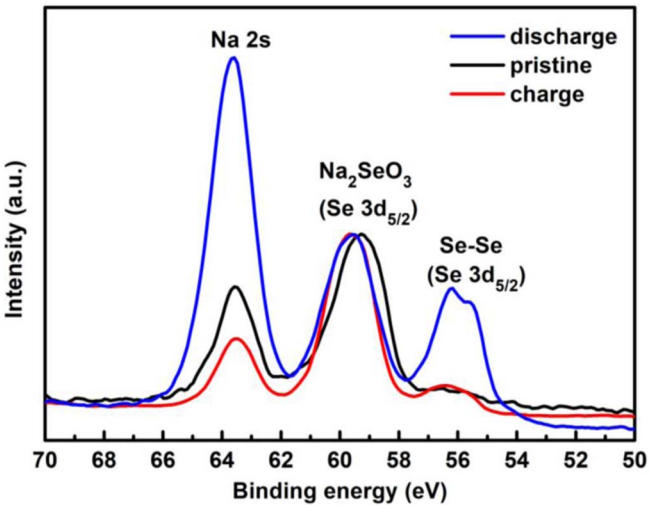


**Figure 3.** XPS spectra of pristine $Na_2SeO_3$ (black), after first charge to 4.9 V (red), after one cycle to 1.5 V (blue).

Downloaded on 2019-07-17 to IP 144.214.124.11 address. Redistribution subject to ECS terms of use (see ecsdl.org/site/terms_use) unless CC License in place (see abstract).

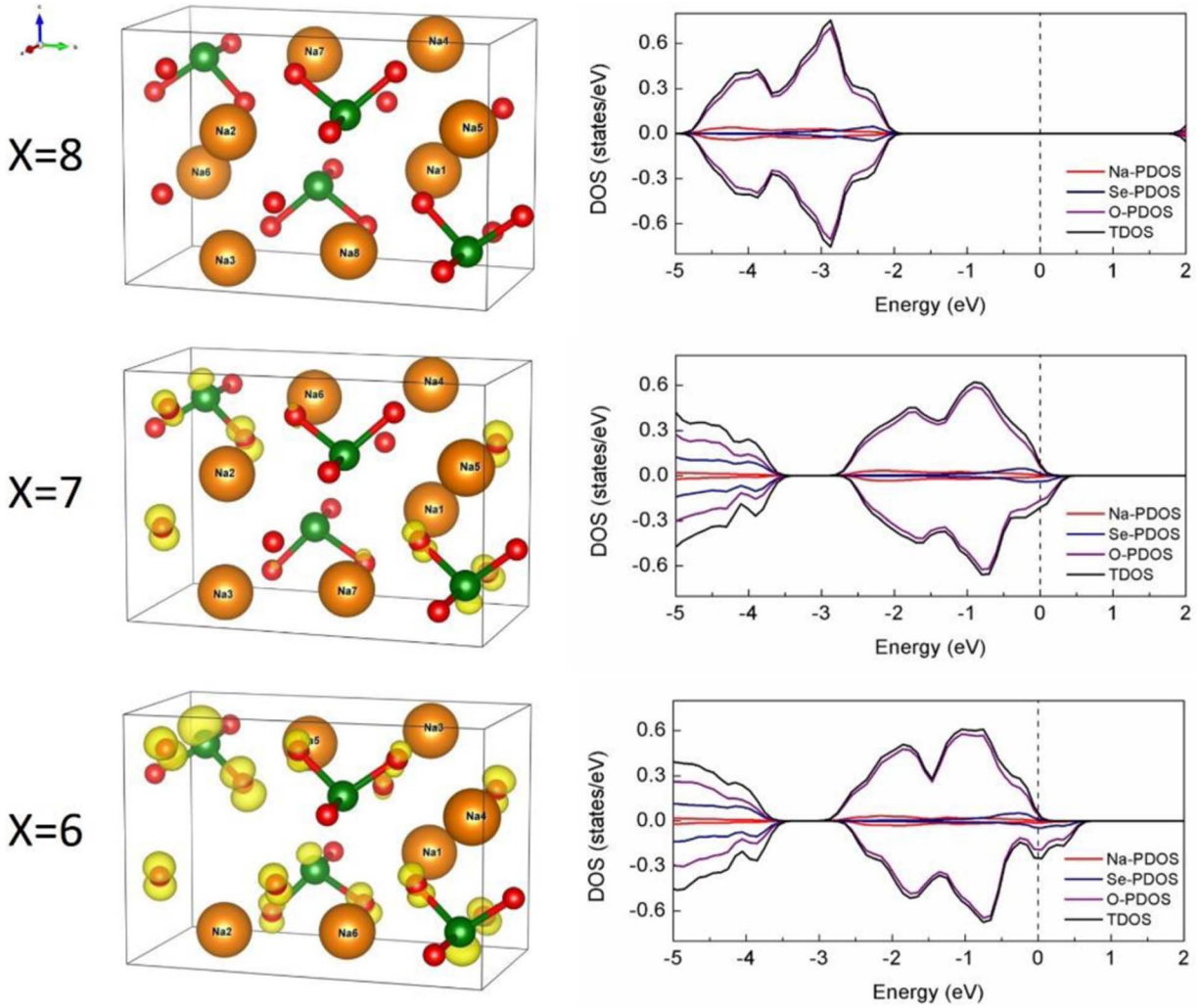


**Figure 4.** Spin density and density of states (DOS) of $Na_xSe_4O_{12}$ unit cell with x = 8, 7 and 6.

***Stability.***—Despite the high capacity, the cycle stability is so far poor. As shown in Fig. 5a, the reversible capacity decreases to 78 mA h $g^{-1}$ after 10 cycles for BM-$Na_2SeO_3$. Ex-situ XRD measurements were carried out on the electrodes after 1st charge at 4.7 V and 1st discharge at 1.5 V. The conditioned coin cells were opened in the glove box and the electrodes were taken out for XRD measurements with Kapton tape to prevent air exposure. Fig. 5b shows that the material becomes amorphous after initial charge and discharge.

After cycling, the appearances of the separator were also observed after opening the coin cells (Figs. 5c–5e). A reddish color can be seen on the Na metal after 3.5 cycles (Fig. 5c). The color intensifies with increasing cycle number. To determine the origin of the reddish color, $Na_2SeO_3$ half cells were assembled with anion exchange membrane (Fumasep FAP450) between two glass fiber separators. After cycling, the separator facing the $Na_2SeO_3$ electrode became reddish whereas the other one facing the Na metal remained white as shown in Fig. 5e. This indicates that the red material comes from the $Na_2SeO_3$ electrode, and its transfer can be hindered by the anion exchange membrane. To further identify the composition of the red material, the red glass fiber separator was washed with DMC and examined with ex-situ Raman spectroscopy without exposing it in air. The result is shown in Fig. 5f. We suspect the red material to be selenium, as the observed peak at 235 $cm^{-1}$ coincide with that of the trigonal phase of selenium.[27] This is also consistent with the appearance of the Se-Se peak in XPS after discharge. Poor cycle stability of the $Na_2SeO_3$ may be the result of the structural degradation and formation of Se together with a reduction of the amount of $Na_2SeO_3$, which is an irreversible and cumulative process.

To improve cycle stability of the material, surface modifications or formation of a surface coating layer with suitable thickness may be possible methods. Positive electrode materials involving oxygen redox reaction tend to have higher surface reactivity, leading to poorer cycle stability. So, the additional surface layer can reduce the contact between the material and electrolyte. There are many examples of surface modifications of Li-rich positive electrode materials, and some of them can be applied to $Na_2SeO_3$.[28,29] Ideally, the surface coating precursor should have good chemical stability and high electrical conductivity since $Na_2SeO_3$ is insulating. Apart from surface coating, doping $Na_2SeO_3$ with elements to stabilize its structure during charge and discharge will likely be necessary as well to improve the electrochemical performance of the material.

## Conclusions

The present study demonstrates for the first time that $Na_2SeO_3$ with an unconventional layered structure can be activated to deliver a high discharge capacity of 232 mAh $g^{-1}$. The unusual capacity is hypothesized to be from oxygen redox reaction, as suggested by XPS and DFT results. Despite the high capacity, cycle performance is currently poor, probably due to structural degradation and selenium dissolution from the materials. Nonetheless, the discovery of a new

Downloaded on 2019-07-17 to IP 144.214.124.11 address. Redistribution subject to ECS terms of use (see ecsdl.org/site/terms_use) unless CC License in place (see abstract).

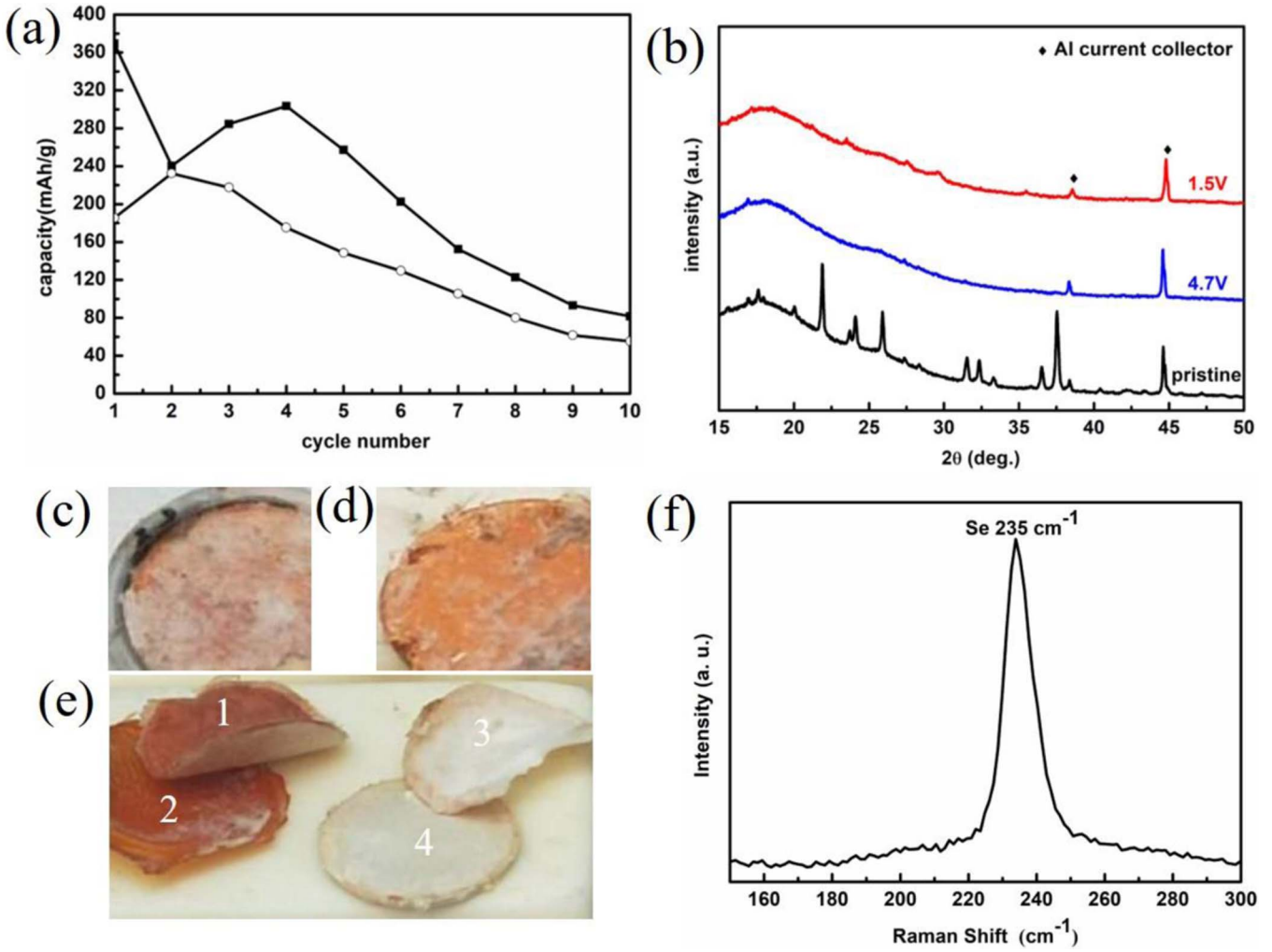


**Figure 5.** (a) Cycle performance of BM-$Na_2SeO_3$ between 1.5–4.7 V at 10 mA $g^{-1}$; (b) XRD profiles of pristine BM-$Na_2SeO_3$ electrodes (black), after initially charge to 4.7 V (blue) and one cycle to 1.5 V (red); (c) appearance of separator on the sodium side after 3.5 cycles; (d) appearance of separator on the sodium side after 7 cycles; (e) appearance of separators after 20 cycles:1-glass fiber separator facing the $NaSeO_3$ electrode, 2-anion-exchange membrane, 3-glass fiber separator facing the sodium side, 4-sodium side; (f) Raman spectroscopy of the red separator after cycling.

sodium-rich material that can give a high capacity can potentially lead to new scientific discovery in the future.

## Acknowledgment

This work was supported by the Research Grants Council (CityU 21202014, CityU 11304518) of the Hong Kong Special Administrative Region, China.

## ORCID

Denis Y. W. Yu https://orcid.org/0000-0002-5883-7087

## References

1. J. Deng, W.-B. Luo, S.-L. Chou, H.-K. Liu, and S.-X. Dou, *Adv. Energy Mater.*, **8**, 1701428 (2018).
2. L. Chen, M. Fiore, J. E. Wang, R. Ruffo, D.-K. Kim, and G. Longoni, *Adv Sustainable Syst.*, **2**, 1700153 (2018).
3. N. Ortiz-Vitoriano, N. E. Drewett, E. Gonzalo, and T. Rojo, *Energy Environ. Sci.*, **10**, 1051 (2017).
4. Y. Li, Y. Lu, C. Zhao, Y.-S. Hu, M.-M. Titirici, H. Li, X. Huang, and L. Chen, *Energy Storage Mater.*, **7**, 130 (2017).
5. L. P. Wang, L. Yu, X. Wang, M. Srinivasan, and Z. J. Xu, *J. Mater. Chem. A*, **3**, 9353 (2015).
6. Z. Jian, W. Han, X. Lu, H. Yang, Y.-S. Hu, J. Zhou, Z. Zhou, J. Li, W. Chen, D. Chen, and L. Chen, *Adv. Energy Mater.*, **3**, 156 (2013).
7. M. Bianchini, N. Brisset, F. Fauth, F. Weill, E. Elkaim, E. Suard, C. Masquelier, and L. Croguennec, *Chem. Mater.*, **26**, 4238 (2014).
8. Z. Lu and J. R. Dahn, *J. Electrochem. Soc.*, **148**, A1225 (2001).
9. X. Xia and J. R. Dahn, *J. Electrochem. Soc.*, **159**, A1048 (2012).
10. Y. Qiao, S. Guo, K. Zhu, P. Liu, X. Li, K. Jiang, C.-J. Sun, M. Chen, and H. Zhou, *Energy Environ. Sci.*, **11**, 299 (2018).
11. A. J. Perez, D. Batuk, M. Saubanère, G. Rousse, D. Foix, E. McCalla, E. J. Berg, R. Dugas, K. H. W. van den Bos, M.-L. Doublet, D. Gonbeau, A. M. Abakumov, G. Van Tendeloo, and J.-M. Tarascon, *Chem. Mater.*, **28**, 8278 (2016).
12. U. Maitra, R. A. House, J. W. Somerville, N. Tapia-Ruiz, J. G. Lozano, N. Guerrini, R. Hao, K. Luo, L. Jin, M. A. Perez-Osorio, F. Massel, D. M. Pickup, S. Ramos, X. Lu, D. E. McNally, A. V. Chadwick, F. Giustino, T. Schmitt, L. C. Duda, M. R. Roberts, and P. G. Bruce, *Nat. Chem.*, **10**, 288 (2018).
13. J. Zhang, B. Su, A. Kitajou, M. Fujita, Y. Cui, M. Oda, W. Zhou, P. H.-L. Sit, and D. Y. W. Yu, *J. Power Sources*, **400**, 377 (2018).
14. D. Ye, G. Zeng, K. Nogita, K. Ozawa, M. Hankel, D. J. Searles, and L. Wang, *Adv. Funct. Mater.*, **25**, 7488 (2015).
15. T. R. Penki, P. K. Nayak, E. Levi, J. Grinblat, Y. Elias, S. Luski, B. Markovsky, and D. Aurbach, *ChemElectroChem*, **5**, 1137 (2018).
16. D. Y. W. Yu, K. Yanagida, Y. Kato, and H. Nakamura, *J. Electrochem. Soc.*, **156**, A417 (2009).
17. N. Yabuuchi, K. Yoshii, S. T. Myung, I. Nakai, and S. Komaba, *J. Amer. Chem. Soc.*, **133**, 4404 (2011).
18. M. H. N. Assadi, M. Okubo, A. Yamada, and Y. Tateyama, *J. Mater. Chem. A*, **6**, 3747 (2018).
19. P. Hohenberg and W. Kohn, *Phys. Rev.*, **136**, B864 (1964).
20. W. Kohn and L. J. Sham, *Phys. Rev.*, **140**, A1133 (1965).

Downloaded on 2019-07-17 to IP 144.214.124.11 address. Redistribution subject to ECS terms of use (see ecsdl.org/site/terms_use) unless CC License in place (see abstract).

21. P. Giannozzi, S. Baroni, N. Bonini, M. Calandra, R. Car, C. Cavazzoni, D. Ceresoli, G. L. Chiarotti, M. Cococcioni, I. Dabo, A. Dal Corso, S. de Gironcoli, S. Fabris, G. Fratesi, R. Gebauer, U. Gerstmann, C. Gougoussis, A. Kokalj, M. Lazzeri, L. Martin-Samos, N. Marzari, F. Mauri, R. Mazzarello, S. Paolini, A. Pasquarello, L. Paulatto, C. Sbraccia, S. Scandolo, G. Sclauzero, A. P. Seitsonen, A. Smogunov, P. Umari, and R. M. Wentzcovitch, *J. Phys. Condens. Matter*, **21**, 395502 (2009).
22. J. P. Perdew, B. Kieron, and M. Ernzerhof, *Phys. Rev. Lett.*, **77**, 3865 (1996).
23. D. Vanderbilt, *Phys. Rev. B*, **41**, 7892 (1990).
24. D. H. Seo, J. Lee, A. Urban, R. Malik, S. Kang, and G. Ceder, *Nat. Chem.*, **8**, 692 (2016).
25. M. S. Wickleder, *Acta Cryst. E*, **58**, i103 (2002).
26. https://srdata.nist.gov/xps/Default.aspx.
27. A. H. Pinto, E. R. Leite, E. Longo, and E. R. de Camargo, *Mater. Lett.*, **87**, 62 (2012).
28. P. K. Nayak, E. M. Erickson, F. Schipper, T. R. Penki, N. Munichandraiah, P. Adelhelm, H. Sclar, F. Amalraj, B. Markovsky, and D. Aurbach, *Adv. Energy Mater.*, **8**, 1702397 (2018).
29. B. Qiu, M. H. Zhang, L. J. Wu, J. Wang, Y. G. Xia, D. A. Qian, H. D. Liu, S. Hy, Y. Chen, K. An, Y. M. Zhu, Z. P. Liu, and Y. S. Meng, *Nat. Commun.*, **7**, 12108 (2016).

Downloaded on 2019-07-17 to IP **144.214.124.11** address. Redistribution subject to ECS terms of use (see **ecsdl.org/site/terms_use**) unless CC License in place (see abstract).